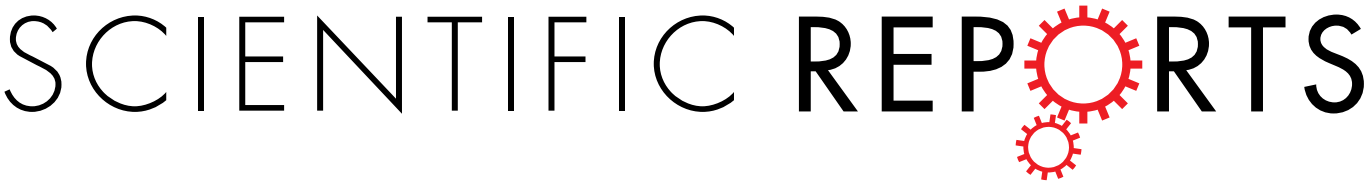

OPEN

Received: 02 March 2016
Accepted: 29 June 2016
Published: 04 August 2016

One-Step Synthesis of Microporous Carbon Monoliths Derived from Biomass with High Nitrogen Doping Content for Highly Selective CO_2 Capture

Zhen Geng[1,2,*], Qiangfeng Xiao[3,*], Hong Lv[1,4], Bing Li[1,4], Haobin Wu[5], Yunfeng Lu[5] & Cunman Zhang[1,4]

The one-step synthesis method of nitrogen doped microporous carbon monoliths derived from biomass with high-efficiency is developed using a novel ammonia (NH_3)-assisted activation process, where NH_3 serves as both activating agent and nitrogen source. Both pore forming and nitrogen doping simultaneously proceed during the process, obviously superior to conventional chemical activation. The as-prepared nitrogen-doped active carbons exhibit rich micropores with high surface area and high nitrogen content. Synergetic effects of its high surface area, microporous structure and high nitrogen content, especially rich nitrogen-containing groups for effective CO_2 capture (i.e., phenyl amine and pyridine-nitrogen) lead to superior CO_2/N_2 selectivity up to 82, which is the highest among known nanoporous carbons. In addition, the resulting nitrogen-doped active carbons can be easily regenerated under mild conditions. Considering the outstanding CO_2 capture performance, low production cost, simple synthesis procedure and easy scalability, the resulting nitrogen-doped microporous carbon monoliths are promising candidates for selective capture of CO_2 in industrial applications.

Carbon capture and sequestration are effective solution for reducing anthropogenic CO_2 emission[1,2]. Since combustion streams, such as flue gas emitted from coal-fired power plants, may comprise ~70% of N_2 and 3–15% of CO_2, selective capture of CO_2 is highly desired[3]. Compared with the conventional amine-scrubbing and pressure-swing adsorption technologies[1,2], selective physisorption techniques are more effective and environmentally friendly. To date, various porous solids, including porous carbons[4–11], metal-organic frameworks (MOFs)[12–14] and covalent organic frameworks (COFs)[15,16] have been extensively studied. Numerous efforts have been focused on optimizing the surface area and pore structure, as well as enhancing their affinity to CO_2 by incorporating various functional groups[4–16]. Various materials with selective CO_2 capture capability have been prepared in laboratory scale; large-scale, low-cost and facile synthesis of materials for effective CO_2 capture, however, remains challenging.

Chemical activation of biomass has been broadly adopted for large-scale and low-cost production of porous carbon materials for a wide range of applications[17–19]. However, such biomass-based carbons generally do not possess sufficient capability for selective adsorption of CO_2[19]. It has been found that incorporating nitrogen (N)-containing groups into carbons (e.g., phenyl amine (Ph-NH_2) and pyridine-N groups) can effectively improve their selective CO_2 capture over N_2 or CH_4, mainly due to the preferred interactions between CO_2 and the electronegative N-containing groups[4–11]. Generally, the doping is achieved by direct activation of N-containing biomass[20–23] or by treating carbons with ammonia[24,25]. For the former approach, the N-containing moieties, however,

[1]Clean Energy Automotive Engineering Center, Tongji University, Shanghai 201804, China. [2]School of Materials Science and Technology, Tongji University, Shanghai 201804, China. [3]Research & Development Center, General Motors, MI 48265-3300, United States. [4]School of Automotive Studies, Tongji University, Shanghai 201804, China. [5]Department of Chemical and Biomolecular Engineering, University of California, Los Angeles, CA 90024, United States. *These authors contributed equally to this work. Correspondence and requests for materials should be addressed to C.Z. (email: zhangcunman@tongji.edu.cn)

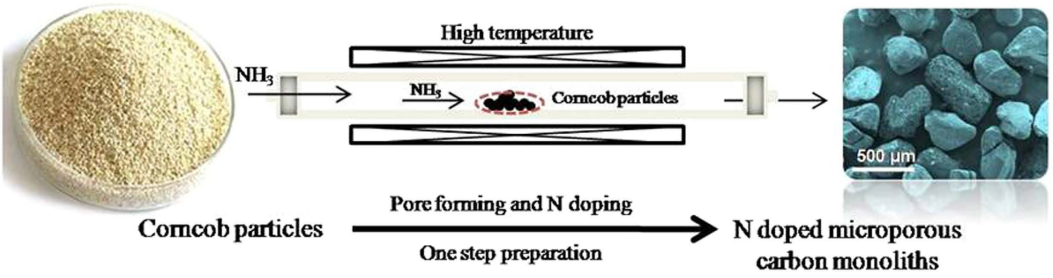

Figure 1. Schematic illustration about one-step synthesis of nitrogen doped microporous carbon monoliths derived from biomass corncob.

are generally volatized during the activation process, resulting in carbons with low N content (e.g., <5 wt%). Similarly, the post-treatment process generally leads to carbons with low N content (e.g., <3 wt%) due to low reaction efficiency between the ammonia and the carbon scaffolds.

We report herein a novel synthesis of N-doped microporous carbon monoliths derived from biomass (corncob) using an ammonia gas (NH_3)-assisted activation process, where NH_3 serves as both the activating agent and the N source. As shown in Fig. 1, corncob particles were efficiently transformed to N-doped microporous carbon monoliths by one-step NH_3-assisted activation process. Both pore forming and nitrogen doping simultaneously proceed during the process, obviously superior to conventional chemical activation. The dual role of NH_3 as the activating agent and N source leads to high surface area, superior pore texture and high N content of the as-prepared carbon materials. To the best of our knowledge, such an NH_3-assisted activation process with high-efficiency has not been reported yet. The resulting N-doped microporous carbon monoliths exhibit excellent selective CO_2 capture performance with excellent CO_2 selectivity over N_2 of 82, which is the highest among reported nanoporous carbons.

Materials and Methods

Sample preparation. Nitrogen-doped active carbons were prepared by a novel chemical activation method using biomass corncob as the carbon source and NH_3 as the activating agent and nitrogen source. Detailed procedures are described as follows. Firstly, after drying for 12 h at 120 °C, corncobs were grounded and sieved into powders with typical size of less than 880 μm. Secondly, the corncob powders were transferred to ceramic boats and heated to 400 °C at 5 °C min^{-1} under N_2 flow of 1.5 L min^{-1} in a horizontal tube furnace to obtain the carbonized particles. Then N_2 was switched to NH_3 and the sample was continued to be heated at 400–800 °C under NH_3 flow of 1.5 L min^{-1}. Then NH_3 was switched back to N_2 when activation was completed and temperature was reduced to 400 °C. Finally, sample was obtained by lowering the temperature to room temperature under N_2 atmosphere. The resulting N-doped active carbons are denoted as NAC-*x*-*y*, where *x* is the activation temperature (°C) and *y* is the activation time (hours) used, respectively.

Corncob-derived activated carbons (CACs) were prepared by KOH chemical activation with biomass corncob as carbon sources and KOH as the activating agent. Detailed procedures are described according to previous reports[17].

Materials characterization and analysis methods. The textural properties of the samples were performed by N_2 sorption at 77 K using a Micromeritics ASAP2020 over a wide relative pressure ranging from about 10^{-6} to 1.0. Prior to the measurements, all samples were degassed at 300 °C for 10 h. The specific surface area (SSA) was assessed by standard BET method (software available in the ASAP2020) using adsorption data in the relative pressure ranging from 0.02 to 0.25. The total pore volume (V_t) was calculated by converting the amount of N_2 adsorbed at a relative pressure of 0.98 to the volume of liquid adsorbate. The micropore volume was calculated by the Dubinine Radushkevich (DR) equation. Pore size distributions (PSDs) were calculated by using the Density Functional Theory (DFT) Plus Software (provided by Micromeritics Instrument Corporation), which is based on calculated adsorption isotherms for pores of different sizes. In the DFT calculations, the equilibrium model of carbon slit-shaped pores with N_2 sorption was applied.

Scanning electron microscope (SEM) and Energy Dispersive Spectrometer (EDS) mapping images were performed on a FEI NOVA Nano electron microscope. Transmission electron microscopy (TEM) and selected area electron diffraction (SAED) were carried out using JEOL JEM-2100F electron microscope. Elemental analysis was obtained by a Thermo Flash EA2000 elemental analyzer. Fourier transform infrared (FT-IR) spectroscopy for samples was analyzed through a BRUKER EQUI NO -XSS spectrometer using the attenuated total reflectance method. X-ray photoelectron spectroscopy (XPS) analysis was performed with an ESCALAB 250Xi spectrometer (Thermo Electron) using a monochromic Al Ka source at 1486.6 eV.

CO_2 and N_2 adsorption performance at ambient pressure was carried out on ASAP2020 adsorption analyzer. All of the samples were evacuated to ultrahigh vacuum at 300 °C for 10 h before the test. CO_2 and N_2 adsorption measurements were performed over the pressure range of 0–1.0 bar at 273 and 298 K, respectively. High purity CO_2 and N_2 (99.999%) were used throughout the tests.

Calculation of CO_2/N_2 selectivity: We calculated the initial slopes of gas uptake for both CO_2 and N_2. The ratio of the slopes was used for calculating the selectivity at 298 K.

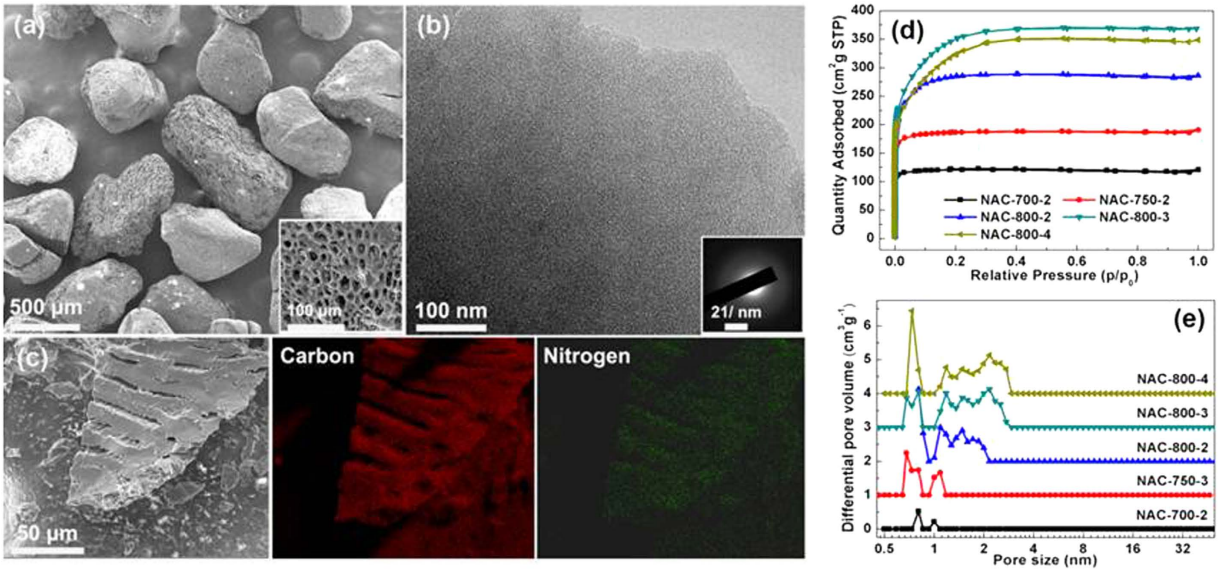

Figure 2. (**a**) SEM images, (**b**) TEM (inset: selected area electron diffraction pattern) and (**c**) EDS mapping images of typical sample NAC-800-3; (**d**) N_2 sorption isotherms and (**e**) Pore size distributions of all NAC samples.

Heat of CO_2 adsorption calculation: The isosteric heat of adsorption (Q_{st}) can be calculated using CO_2 adsorption isotherms measured at different temperatures based on the Clausius-Clapeyron equation (Eq. 1):

$$\ln\left(\frac{P_2}{P_1}\right) = \frac{Q_{st}}{R}\left(\frac{1}{T_1} - \frac{1}{T_2}\right) \quad (1)$$

where P_i is pressure for isotherm i; T_i is temperature for isotherm i; R is the universal gas constant 8.315 J K^{-1} mol^{-1}. In this study, the Q_{st} was calculated using CO_2 adsorption isotherms measured at 273 and 298 K.

Results and Discussion

Figure 2 shows scanning electron microscope (SEM) and transmission electron microscopy (TEM) images of a typical sample (NAC-800-3). It presents the monolith shape with an average size of 0.5–1 mm in diameter (Fig. 2a), which would be more advantageous over smaller-size sorbents for practical applications[4]. The skeleton of these monoliths exhibits a honeycomb-like structure with interconnected macropores of ~15 μm in diameter (inset of Fig. 2a). Such pore structure is also advantageous for CO_2 sorption with low transport resistance[5]. TEM image (Fig. 2b) suggests that the carbon contains uniform micropores. The electron diffraction of the sample shows an amorphous structure (inset of Fig. 2b), which is consistent with most of the activated carbons derived from biomass.

Figure 2c further shows a SEM image of a NAC sample along with its element mapping. Noticeably, N is homogenously distributed within the carbon framework. Elemental analysis (Table 1) shows negligible amount of N in natural corncob and its directly carbonized product. Meanwhile, activation in NH_3 can easily dope N into carbon framework even at 400 °C, although it is difficult to form a porous structure at such a low temperature. Further increase of the activation temperature leads to increase of N content, reaching ~12 wt% at 800 °C, which is unsurpassable for all existing chemical activation methods (e.g., 5.11 at% for HHC[21]; 4.84 wt% for PA-400-KOH-1-600[23]; 8.1 wt% for CN700[24]; 9.2 wt% for CNO300[26]; 4.5 wt% for AN[27]).

Such high N content is comparable with those made from specially designed compounds that require highly complex chemical synthesis (e.g., 10.14 wt% for CP-2-600[5]; 12.9 wt% for IBN9-NCI-A[8]; 11.95 wt% for PPN-6-CH_2DETA[14]). The increasing trend of N doping with increasing temperature is different from literatures, where the content of N doping generally decreases with increasing temperature, particularly, when temperature is above 500 °C due to high volatility of the N-containing species[6,28]. The continuous increase of the N content implies a dynamic balance of N doping and removal during the reactions, where the rate of N doping into carbon is over that of N removal from carbon. This method provides a direct approach to fabricate highly N-doped carbons simply by activating biomass in NH_3 atmosphere.

Figure 2d shows N2 sorption isotherms of the samples prepared at different activation temperature and time, which exhibit type I isotherms with typical microporous structure[20]. With increasing the activation temperature from 400 to 800 °C, isotherms with significantly increased pore volume accompanied with enlarged pore sizes are obtained. As shown in Table 1, NAC-400-2, NAC-500-2, and NAC-600-2 show insignificant value of specific surface area (SSA), implying a poor activation at temperature below 600 °C. SSA gradually increases with increasing activation temperature and time, reaching a maximum of 1154 m^2 g^{-1} with an activation temperature of 800 °C for 3 hours (NAC-800-3). Figure 2e further shows the pore size distributions calculated based on DFT model,

Samples	Pore properties			Elemental analysis			Yield(wt%)
	SSA[a] (m^2g^{-1})	V_t[b] (cm^3g^{-1})	C(wt%)	N(wt%)	O(wt%)	H(wt%)	
Corncob	–	–	44.87	0.38	48.43	6.32	–
Carbonized particle	–	–	75.15	<0.3	20.2	4.35	–
CAC	3711	2.07	91.63	<0.3	7.39	0.38	32.34
NAC-400-2	–	–	78.80	1.47	16.59	3.14	86.8
NAC-500-2	–	–	82.44	1.82	12.90	2.84	77.68
NAC-600-2	–	–	83.70	3.88	10.37	2.05	78.04
NAC-700-2	494	0.16	78.21	9.82	9.16	1.41	77.21
NAC-750-2	784	0.27	78.11	10.59	9.84	1.46	67.63
NAC-800-2	1086	0.44	75.43	10.82	12.29	1.46	45.24
NAC-800-3	1154	0.57	69.10	11.52	17.88	1.50	27.62
NAC-800-4	1027	0.53	65.67	12.30	20.52	1.91	17.13

Table 1. Textural and chemical characteristic of various samples. [a]SSA, specific surface area calculated by BET equation at $P/P_o = 0.02–0.25$. Correlation coefficient of BET curves for all samples is higher than 0.9999. [b]V_t, total pore volume estimated from the adsorption amount of N_2 at $P/P_o = 0.98$.

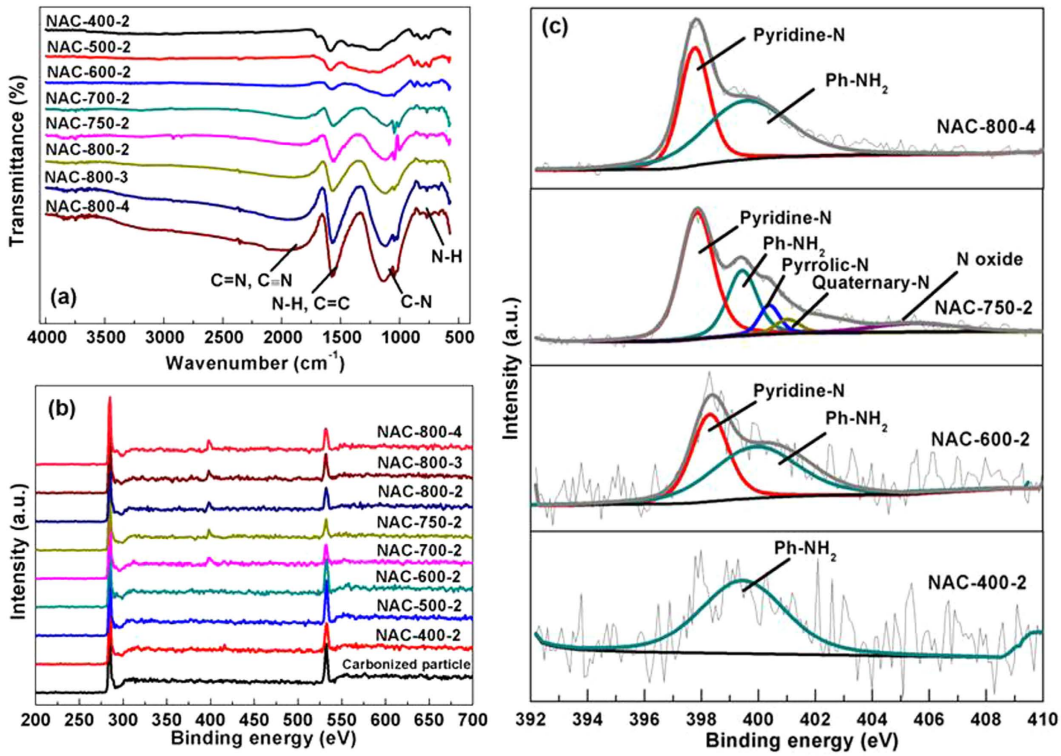

Figure 3. (**a**) FT-IR and (**b**) XPS spectra of all NAC samples; (**c**) N 1s XPS spectra of NAC-400-2, NAC-600-2, NAC-750-2 and NAC-800-4.

which shows enlarged pore diameter and broadened distribution along with increasing activation temperature and time. The pore size distribution of NAC-800-4 is similar to porous carbons prepared by KOH activation[17–19]. These samples contain a large fraction of micropores ranging from 0.8 to 1 nm in diameter, as well as mesopores below 4 nm. Combining with the macroporous structure, such carbons with high-level of N-doping and hierarchically porous structure are of great interest for sorption and other applications.

The nature of N within the carbons is investigated by Fourier transform infrared (FT-IR) spectra and X-ray photoelectron spectroscopy (XPS). FT-IR spectra (Fig. 3a) of samples shows a board band at 2000 cm^{-1}, which is characteristic of the nitrile group or C=N from pyridine and quinoline[29,30]. The bands at ca. 1590 cm^{-1} can be assigned to the presence of N-H in-plane deformation vibration or C=C stretching vibration from aromatic rings[6]. The peaks around 1150–900 cm^{-1} are attributed to the C-N stretching vibration. The broad weak bands between 950 and 650 cm^{-1} correspond to out-of-plane N-H deformation vibration[5,6]. Hence, FT-IR analysis confirms the existence of numerous N-containing groups in the carbon samples.

Besides, XPS spectra of NACs (Fig. 3b) clearly shows the incorporation of N atoms into carbon framework. The bonding configurations of N atoms are further characterized by the high-resolution N1s spectra (Fig. 3c). The peaks of N1s spectra can be deconvolved and assigned to various N-containing groups, including pyridine N (398.1 eV), Ph-NH_2 (399.4 eV), pyrrolic N (400.5 eV), quaternary N (401.3 eV) and N-oxides (402–405 eV)[5–8,31]. As shown in Fig. 3c, N-containing species within the samples change significantly with activation temperature and time. Specifically, only one peak corresponding to Ph-NH_2 group (399.4 eV) can be seen at a low activation temperature (NAC-400-2). Two intense peaks at 398.3 and 399.7 eV can be distinguished above 600 °C, corresponding to pyridine-N and Ph-NH_2 respectively. During the activation at 750 °C, multiple N species are formed, including pyridine-N, Ph-NH_2, pyrrolic-N, quaternary-N and N-oxides. However, most of N-containing groups are highly volatile at high temperature. With further increased temperature and reaction time, only two N-containing groups, i.e., pyridine-N and Ph-NH_2 remain at 800 °C (Figure S1). Noticeably, Ph-NH_2 and pyridine-N are the most effective N-containing groups for CO_2 capture due to the preferred interactions between CO_2 and the electronegative N-containing groups[4–11].

From the thermodynamic point of view, the direct reaction between carbon and NH_3 (Eq. 2),

$$NH_3(g) + C \rightarrow HCN(g) + H_2(g) \quad (2)$$

is favorable only at high temperature (e.g., $\triangle H = 188.53\ kJ\ mol^{-1}$ at 1273 K)[32,33]. The ability to realize high-level of N-doping at low temperature can be attributed to the unique chemical composition of the corncob precursor. The main compositions of corncob are cellulose, hemicellulose and lignin[34,35], possessing multiple oxygen (O)-containing groups, e.g., C–O, C=O and –OH etc., which can be identified at 900–1800 cm^{-1} in the FT-IR spectrums (Figure S2). Such groups may play important roles for N doping during NH_3 treatment[24,27]. As shown in Table 1, large amounts of the O-containing groups are consumed during the initial activation process, as suggested by the obvious decrease of the O content. It is possible that NH_3 reacts with such groups, forming amine-containing sites such as Ph-NH_2 moieties. With increase of the activation temperature, the carbon scaffolds react with NH_3, forming pores by transforming carbon to Hydrogen cyanide gas (HCN)[32,33], during which N atoms are also doped into the aromatic rings (e.g., in the forms of C–N or C=N). As a result, the N content continually increases, accompanied by the decrease content of carbon with increasing the degree of the activation.

To confirm the role of the O-containing groups in the doping process, corncob-derived activated carbon (denoted as CAC, SSA of ~3711 m^2g^{-1}) is also prepared by the conventional KOH activation method (see preparation details in Experimental Section). Such carbon materials contain significantly lower content of the O-containing groups (~ 7% vs ~20% for the pre-carbonated corncob particles, see Table 1 and Figure S2). Consistently, treating the CAC by NH_3 under the same condition leads to a much lower N doping (<2%) even at 800 °C, confirming the essential roles of the O-containing groups in the N-doping process. Based on the studies presented, it is reasonable to conclude that NH_3 plays dual roles as the activating agent and N-doping source. During the activation process, such N-containing groups are dynamically generated and removed, leading to the formation of highly porous carbons with high content of Ph-NH_2 and pyridine-N groups.

Figure 4a shows the CO_2 adsorption performance of as-prepared samples at 1 bar and 298 K. Remarkably, CO_2 adsorption capacity improves with increased activation temperature and slightly increased reaction time, reaching a maximum value of 2.81 mmol g^{-1} for NAC-800-3 due to the high SSA and large amount of N-containing groups (i.e. Ph-NH_2 and pyridine-N). For comparison, CAC is also tested for CO_2 adsorption. Interestingly, although NAC-800-3 only holds one third of SSA of CAC, its CO_2 adsorption capacity is about 33% higher, which reveals the crucial role of N-containing groups on CO_2 capture.

More importantly, the N-containing groups also endow NACs with advantages on CO_2/N_2 selectivity. Adsorption selectivity of CO_2 over N_2 is calculated by the ratio of initial slopes of the CO_2 and N_2 adsorption isotherms (Figure S3 and Figure S4). As a result, the CO_2/N_2 selectivity of representative sample NAC-800-3 is about 82:1 at 298 K. To the best of our knowledge, such CO_2/N_2 selectivity is one of the highest values among reported nanoporous carbons (e.g., 28 for HCM-DAH-1[4], 42 for IBN9-NCI[8], 59 for CPC 550[9], 124 for SU-MAC-500[36]). In addition, the ideal adsorption solution theory (IAST) selectivity (assuming gas mixture of CO_2/N_2 with 10% CO_2 at 1 bar) is calculated to be 45:1 at 298 K. The value discrepancy between the initial slope method and IAST method can be attributed to the adsorption site heterogeneity[37]. As shown in Fig. 4d, although higher CO_2/N_2 selectivity has been achieved on other porous framework materials (e.g., 140 for SIFSIX-Cu-I at 298 K[13], 442 for PPN6-CH_2DETA at 298 K[14], 288 for azo-COP at 323 K[15]), considering the low-cost, easy scalability and facile synthesis method, the NACs reported in this work are more attractive for potential industrial applications.

Superior CO_2/N_2 selectivity of NAC-800-3 is also supported by ultra-high isosteric heats of adsorption (Q_{st}). Q_{st} can be calculated via the CO_2 adsorption isotherms at 273 and 298 K (Fig. 4b,c) and applying the Clausius-Clapeyron equation (E.g. 1, see calculation details in the Experimental Section). NAC-800-3 exhibits an ultra-high Q_{st} of 55.1 kJ mol^{-1} at the initial stage and 30.5 kJ mol^{-1} at the steady stage (Fig. 5a), which is much higher than those previously reported values of porous carbons (e.g., 35.9–21.1 kJ mol^{-1} for HCM-DAH-1[4], 44.1–27.0 kJ mol^{-1} for IBN9-NCI[8]). As a comparison, N-free CAC exhibits a lower and almost unchanged Q_{st} of 28.9–24.4 kJ mol^{-1}. The ultra-high Q_{st} of NAC-800-3 at the initial stage decreases gradually at higher uptake, which indicates the presence of active sites (i.e., N-containing groups) on the surface of NAC[38].

Overall, both surface chemical property (i.e. N-containing groups) and high SSA accompanied with microporous structure are critically important for selective adsorption of target gas molecules. Although CAC is essentially microporous and possesses ultra-high SSA, it only exhibits low selectivity of about 7:1 (Fig. 4c and Figure S4), which is obviously inferior to NAC-800-3. Hence, merely increasing SSA of carbon adsorbent is not enough for enhancing selective CO_2 capture performance. The ultra-high Q_{st} of NAC-800-3 is due to the synergetic effects of high SSA with microporous structure and rich N-containing groups, leading to superior selective adsorption of CO_2 over N_2.

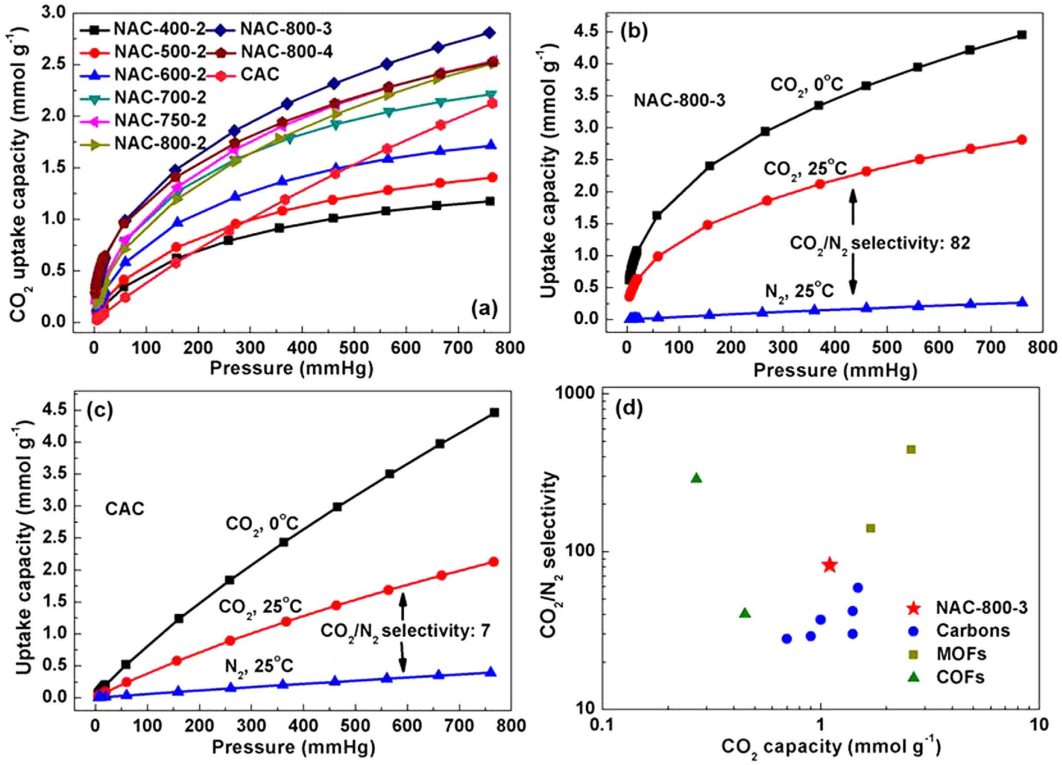

Figure 4. (**a**) CO_2 adsorption isotherms of all NAC samples at 1 bar and 298 K; (**b**) Adsorption isotherms of NAC-800-3 for CO_2 at 273 and 298 K, and N_2 at 298 K; (**c**) Adsorption isotherms of CAC for CO_2 at 273 and 298 K, and N_2 at 298 K; (d) Comparison of CO_2 adsorption capacity (298 K, 0.1 bar) and CO_2/N_2 selectivity of NAC-800-3 with different types of representative solid physisorbents (carbons[4–11], MOFs[12–14], COFs[15,16]).

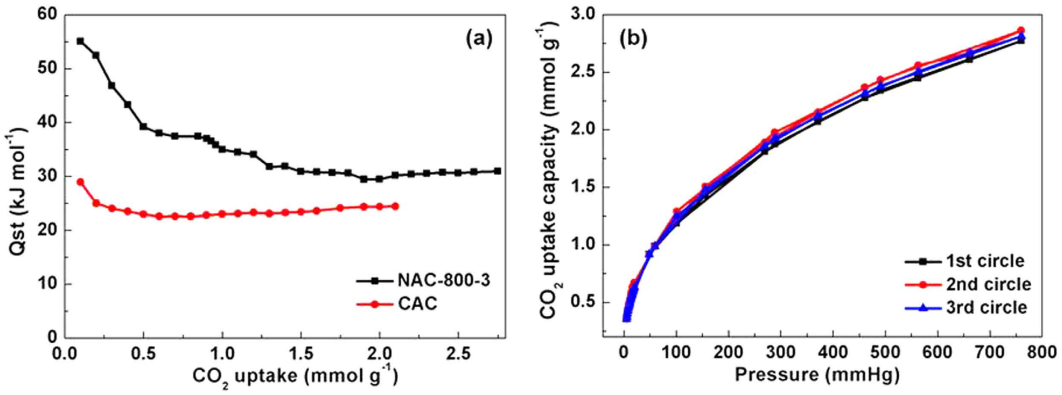

Figure 5. (**a**) Isosteric heat of CO_2 adsorption for NAC-800-3 and CAC at different CO_2 uptakes; (**b**) CO_2 multi-circle sorption isotherms for NAC-800-3 at 298 K.

The reversibility of CO_2 adsorption for NAC-800-3 at 298 K has been tested over 3 cycles (Fig. 5b). Adsorption capacities for 3 cycles are almost identical, with generally overlapped desorption and adsorption curves. Thus, CO_2 capture in NAC is highly reversible and primarily based on physisorption. The easy regeneration of NAC under mild conditions makes it superior to aqueous amine and amine-modified solids, which require large amount of energy during the regeneration process[1,2].

Conclusion

In summary, we have developed a one-step synthesis method of N-doped microporous carbon monoliths derived from biomass using an NH_3-assisted activation process, where NH_3 serves as both activating agent and N source. The as-prepared N-doped active carbons (NACs) exhibit rich micropores with high surface area and high N content. Synergetic effects of its high surface area, microporous structure and high N content, especially rich N-containing groups for effective CO_2 capture (i.e., Ph-NH_2 and pyridine-N) lead to superior CO_2/N_2 selectivity up to 82, which is the highest among known nanoporous carbons. In addition, the NACs can be easily regenerated

under mild conditions. Considering the outstanding CO_2 capture performance, low production cost, simple synthesis procedure and easy scalability, NACs are promising candidates for selective capture of CO_2 in industrial applications.

References

1. D'Alessandro, D. M., Smit, B. & Long, J. R. Carbon dioxide capture: prospects for new materials. *Angew. Chem. Int. Ed.* **49,** 6058–6082 (2010).
2. Rochelle, G. T. Amine scrubbing for CO_2 capture. *Science* **325,** 1652–1654 (2009).
3. Lee, K. B. & Sircar, S. Removal and recovery of compressed CO_2 from flue gas by a novel thermal swing chemisorption process. *AIChE J.* **54,** 2293–2302 (2008).
4. Hao, G. P. *et al.* Structurally designed synthesis of mechanically stable poly(benzoxazine-co-resol)-based porous carbon monoliths and their application as high-performance CO_2 capture sorbents. *J. Am. Chem. Soc.* **133,** 11378–11388 (2011).
5. Sevilla, M., Valle-Vigon, P. & Fuertes, A. B. N-doped polypyrrole-based porous carbons for CO_2 capture. *Adv. Funct. Mater.* **21,** 2781–2787 (2011).
6. Hao, G. P., Li, W. C., Qian, D. & Lu, A. H. Rapid synthesis of nitrogen-doped carbon monolith for CO_2 capture. *Adv. Mater.* **22,** 853–857 (2010).
7. Wang, L. & Yang, R. T. Significantly increased CO_2 adsorption performance of nanostructured templated carbon by tuning surface area and nitrogen doping. *J. Phys. Chem. C* **116,** 1099–1106 (2012).
8. Zhao, Y. F. *et al.* Novel porous carbon materials with ultrahigh nitrogen contents for selective CO_2 capture. *J. Mater. Chem.* **22,** 19726–19731 (2012).
9. Ashourirad, B., Sekizkardes, A. K., Altarawneh, S. & El-Kaderi, H. M. Exceptional gas adsorption properties by nitrogen-doped porous carbons derived from benzimidazole-linked polymers, *Chem. Mater.* **27,** 1349–1358 (2015).
10. Wei, J. *et al.* A controllable synthesis of rich nitrogen-doped ordered mesoporous carbon for CO_2 capture and supercapacitors. *Adv. Funct. Mater.* **23,** 2322–2328 (2013).
11. Ma, X. Y., Cao, M. H. & Hu, C. W. Bifunctional HNO_3 catalytic synthesis of N-doped porous carbons for CO_2 capture. *J. Mater. Chem.* A **1,** 913–918 (2013).
12. Luo, F. *et al.* Photoswitching CO_2 capture and release in a photochromic diarylethene metal–organic framework. *Angew. Chem. Int. Ed.* **53,** 9298–9301 (2014).
13. Nugent, P. *et al.* Porous materials with optimal adsorption thermodynamics and kinetics for CO_2 separation. *Nature* **495,** 80–84 (2013).
14. Lu, W. G. *et al.* Polyamine-tethered porous polymer networks for carbon dioxide capture from flue gas. *Angew. Chem. Int. Ed.* **51,** 7480–7484 (2012).
15. Patel, H. A. *et al.* Unprecedented high-temperature CO_2 selectivity in N_2-phobic nanoporous covalent organic polymers. *Nature Commun.* **4,** 1357–1364 (2013).
16. Gao, X., Zou, X. Q., Ma, H. P., Meng, S. & Zhu, G. S. Highly selective and permeable porous organic framework membrane for CO_2 Capture. *Adv. Mater.* **26,** 3644–3648 (2014).
17. Zhang, C. M. *et al.* Microstructure regulation of super activated carbon from biomass source corncob with enhanced hydrogen uptake. *Int. J. Hydrogen Energy* **38,** 9243–9250 (2013).
18. Wang, J. C. & Kaskel, S. KOH activation of carbon-based materials for energy storage. *J. Mater. Chem.* **22,** 23710–23725 (2012).
19. Lu, A. H., Hao, G. P. & Zhang, X. Q. In *Porous Materials for Carbon Dioxide Capture* (ed. Lu, A. H. & Dai, S.) Ch. 2, 15–78 (Springer, Verlag Berlin Heidelberg, German, 2014).
20. Xu, G. Y. *et al.* Biomass-derived porous carbon materials with sulfur and nitrogen dual-doping for energy storage. *Green Chem.* **17,** 1668–1674 (2015).
21. Saravanan, K. R. & Kalaiselvi, N. Nitrogen containing bio-carbon as a potential anode for lithium batteries. *Carbon* **81,** 43–53 (2015).
22. Wang, J. C. *et al.* Fungi-based porous carbons for CO_2 adsorption and separation. *J. Mater. Chem.* **22,** 13911–13913 (2012).
23. Song, J., Shen, W. Z., Wang, J. G. & Fan, W. B. Superior carbon-based CO_2 adsorbents prepared from poplar anthers. *Carbon* **69,** 255–263 (2014).
24. Pevida, C. *et al.* Surface modification of activated carbons for CO_2 capture. *Appl. Surf. Sci.* **254,** 7165–7172 (2008).
25. Przepiorski, J., Skrodzewicz, M. & Morawski, A. W. High temperature ammonia treatment of activated carbon for enhancement of CO_2 adsorption. *Appl. Surf. Sci.* **225,** 235–242 (2004).
26. Plaza, M. G., Rubiera, F., Pis, J. J. & Pevida, C. Ammoxidation of carbon materials for CO_2 capture. *Appl. Surf. Sci.* **256,** 6843–6849 (2010).
27. Plaza, M. G., García, S., Rubiera, F., Pis, J. J. & Pevida, C. Evaluation of ammonia modified and conventionally activated biomass based carbons as CO_2 adsorbents in postcombustion conditions. *Sep. Sci. Technol.* **80,** 96–104 (2011).
28. Weidenthaler, C., Lu, A. H., Schmidt, W. & Schuth, F. X-ray photoelectron spectroscopic studies of PAN-based ordered mesoporous carbons (OMC). *Micropor. Mesopor. Mater.* **88,** 238–243 (2006).
29. Senthilnathan, J., Liu, Y. F., Rao, K. S. & Yoshimura, M. Submerged liquid plasma for the synchronized reduction and functionalization of grapheme oxide. *Sci. Rep.* **4,** 4395–4401 (2014).
30. Méndez-Ardoy, A., Steentjes, T., Kudernac, T. & Huskens, J. Self-assembled monolayers on gold of β-cyclodextrin adsorbates with different anchoring groups. *Langmuir* **30,** 3467–3476 (2014).
31. Horikawa, T. *et al.* Preparation of nitrogen-doped porous carbon by ammonia gas treatment and the effects of N-doping on water adsorption. *Carbon* **50,** 1833–1842 (2012).
32. Sherwood, T. K. & Maak, R. O. The reaction of ammonia with carbon at elevated temperatures. *Ind. Eng. Chem. Fundamen.* **1(2),** 111–115 (1962).
33. Shevlin, P. B., McPherson, D. W. & Melius, P. Reaction of atomic carbon with ammonia. The mechanism of formation of amino acid precursors. *J. Am. Chem. Soc.* **105(3),** 488–491 (1983).
34. Sych, N. V. *et al.* Porous structure and surface chemistry of phosphoric acid activated carbon from corncob. *Appl. Surf. Sci.* **261,** 75–82 (2012).
35. Bu, L. X., Tang, Y., Gao, Y. X., Jian, H. L. & Jiang, J. X. Comparative characterization of milled wood lignin from furfural residues and corncob. *Chem. Eng. J.* **175,** 176–184 (2011).
36. To, J. W. F. *et al.* Hierarchical N-doped carbon as CO_2 adsorbent with high CO_2 selectivity from rationally designed polypyrrole precursor. *J. Am. Chem. Soc.* **138(3),** 1001–1009 (2016).
37. Ruthven, D. M. *Principles of adsorption and adsorption processes.* John Wiley & Sons, 1984).
38. Xia, Y. D., Walker, G. S., Grant, D. M. & Mokaya, R. Hydrogen storage in high surface area carbons: experimental demonstration of the effects of nitrogen doping. *J. Am. Chem. Soc.* **131,** 16493–16499 (2009).

Acknowledgements

The authors would like to acknowledge the support from the National High Technology Research and Development Program of China (863 Program, 2012AA0053301).

Author Contributions

Z.G. amd C.Z. conceived the experiments; Z.G. conducted the experiments; H.L. and B.L. provided assistance in testing and analysis; Z.G. analyzed the data and wrote the manuscript; Q.X., H.W. and Y.L. edited and revised the manuscript. All authors reviewed the manuscript.

Additional Information

Supplementary information accompanies this paper at http://www.nature.com/srep

Competing financial interests: The authors declare no competing financial interests.

How to cite this article: Geng, Z. *et al.* One-Step Synthesis of Microporous Carbon Monoliths Derived from Biomass with High Nitrogen Doping Content for Highly Selective CO_2 Capture. *Sci. Rep.* **6**, 30049; doi: 10.1038/srep30049 (2016).